JOURNAL OF MATERIALS SCIENCE 19 (1984) 815–837

Corrosion in H_2/H_2S mixtures of a $Ni_{77}Cr_{16}Fe_7$ alloy previously covered with an external Cr_2O_3 layer

G. MOULIN, M. AUCOUTURIER, P. LACOMBE
Laboratoire de Metallurgie Physique, LA 177, Bâtiment 413, Université de Paris XI, 91405 Orsay Cedex, France

A thermodynamic and kinetic study of sulphidization of $Ni_{77}Cr_{16}Fe_7$ alloys – previously covered with a Cr_2O_3 layer – was made in a H_2/H_2S mixture, under a wide range of sulphur pressures (10^{-4} atm $< p(H_2S) < 10^{-1}$ atm) and at temperatures between 700 and 1000° C. The mechanism for sulphur penetration through the external chromium oxide and the competition between Cr_2O_3 reduction and CrS formation were studied with the help of thermogravimetry and analytical techniques. The essential role of chromium carbides appears to be to modify the distribution of sulphur in the structure and to lower the critical energy for sulphide formation. Two growth laws were found to apply for external layer formation, one for the industrial form of the alloy and the other for a purer synthetic form. The alteration in mechanical properties of the external sulphidized zone were used to show the initial softening effect of chromium depletion, then the hardening effect of sulphide precipitation.

1. Introduction

The oxidation mechanisms of chromium-containing alloys have been thoroughly studied and discussed [1, 2]. The situation is very different for sulphidation. The general action of sulphur-containing atmospheres on Ni–Cr base alloys appears to be very different from that of pure oxidizing atmospheres [3, 4]. In previous papers the quantitative behaviour of 77Ni–16Cr–7Fe alloys was described from the view-point of:

1. sulphide-forming penetration and surface-scale formation under H_2S/H_2 atmospheres with $p(H_2S) \geqslant 10^{-4}$ atm [5];

2. atomic bulk and grain boundary diffusion of sulphur in the alloy [6];

3. interaction of sulphur with microstructural defects, and microsulphide nucleation [7].

In order to make further progress in a complete description of the sulphidizing processes of these alloys and to propose a general mechanism taking into account the possible existence of a pre-existing oxide surface film, it is necessary to acquire results on the very first stages of attack by H_2S/H_2 atmospheres. This stage begins with a dissociative adsorption of H_2S into H^+ and S^{2-} [8]. A comprehensive literature analysis [9] shows up a lack of information which arises from:

1. The absence of genuine data concerning the dissolution of sulphur in the surface layers of any alloy: the nickel and cobalt oxides usually studied are much less stable than Cr_2O_3 and, in the former, reduction phenomena are favoured, so that the predominant mechanism is more likely a sulphur adsorption on nickel and cobalt crystallites [10]. Paradoxically, the stability of Cr_2O_3-type oxides in H_2/H_2S mixture is very high [11], but sulphur dissolution in these oxides has not been analysed.

2. The impossibility of discriminating the true surface reaction process from the bulk penetration during a sulphur attack experiment. These processes are simultaneous when the sulphidizing conditions are severe (high partial pressure or high temperature).

The purpose of this paper is to take advantage of published [5–7] and unpublished quantitative results obtained on the sulphur attack processes

0022–2461/84 $03.00 + .12

of an Inconel alloy under controlled thermodynamic conditions, to propose a complete mechanistic description of all the steps of the sulphidization of the alloy. These steps will be described and discussed by following a logical order:

1. atomic sulphur penetration into the surface layer and in the metal;

2. sulphur atoms gathering as clusters or two-dimensional compounds on the surface and in the metal;

3. nucleation of chromium sulphides on the surface and in the bulk of the metal;

4. growth of the sulphide phases on the surface and in the bulk of the metal.

For the sake of clarity, strong emphasis is placed on the results obtained for low-pressure atmospheres, $p(H_2S)$ (10^{-5} to 10^{-4} atm), and low temperatures (700° C).

2. Experimental techniques and materials

2.1. Experimental techniques

The sulphidation kinetics must be measured in a thermodynamically-controlled atmosphere allowing very low sulphur potentials if necessary. The sulphidizing (H_2/H_2S) device has been described in other publications [5, 12]. H_2S pressures ranging from 10^{-2} to 10^{-5} atm are produced by thermal decomposition of Cu_2S (or Ag_2S) under 0.4 atm H_2.

A Cahn microthermobalance (± 2 μg sensitivity), directly connected to the H_2/H_2S producing device (Fig. 1), allows quantitative kinetic measurements from 650 to 1200° C.

The determination of sulphur distribution in the microstructure of the alloy has been made by two different techniques:

1. High-resolution autoradiography [6, 13] is used to locate radioactive ^{35}S introduced by diffusion: the specimen (massive or thin foil) is coated with a protective layer and a monolayer of AgBr grains (Fig. 2a) (Ilford L_4 emulsion). After development (D 19B developer) and fixing, the presence of sulphur atoms is revealed by silver filament.

2. The high-resolution sulphur (Baumann) microprint technique is able to show sulphur-gathering, using the specificity of the ancient "Baumann Test" (sulphur print test) and the excellent resolution of high resolution nuclear emulsions [7, 14]: the AgBr layer is directly deposited on the specimen or thin foil surface and

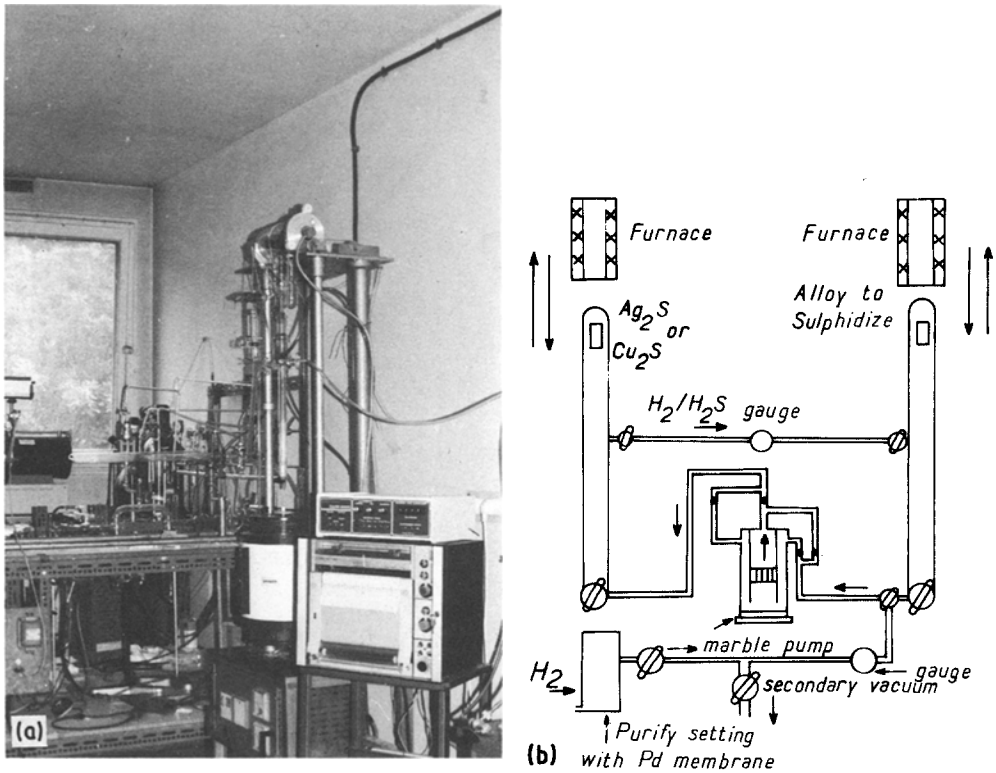

Figure 1 H_2/H_2S treatment device.

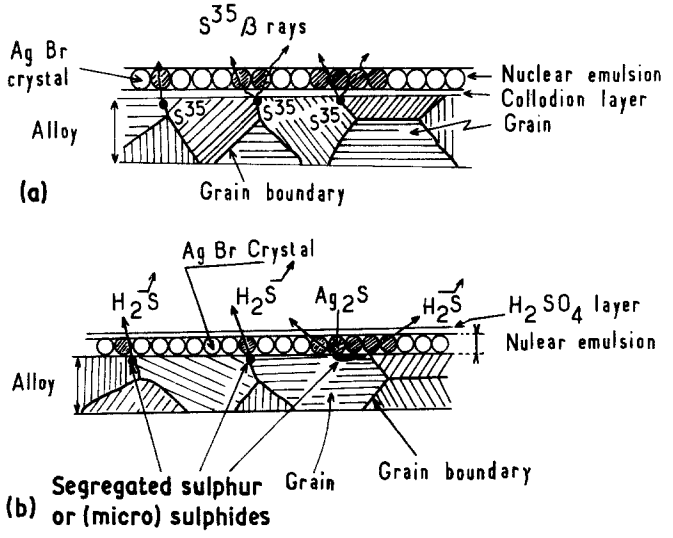

Figure 2 (a) High resolution sulphur autoradiography. (b) High resolution Baumann microprint.

wetted with a thin H_2SO_4 film (Fig. 2b). From the usual chemical reaction of sulphide displacement and AgBr reduction by the produced H_2S, the AgBr grains are transformed into spherical Ag_2S grains. After fixing, the Ag_2S spheres indicate specifically the presence of microsulphide. The technique is sensitive to the equivalent of a two-dimensional compound, according to recent comparative studies with Auger spectrometry [15]. The other experimental techniques are more usual although used extensively: optical microscopy, scanning or transmission electron microscopy, Auger electron spectroscopy, tensile testing (at 20 and $-196°C$, and $v = 1.5 \times 10^{-3}\,sec^{-1}$) electrochemical measurements (potentio-kinetic curves in 20% H_2SO_4, $2\,V\,h^{-1}$).

2.2. Materials and heat treatments

An industrial alloy, with the composition given in Table I, has been investigated, as well as pure synthetic alloy, containing 30 ppm carbon, 200 ppm oxygen, 20 ppm nitrogen; the principal other impurities being aluminium (1000 ppm) and titanium (3000 ppm).

Before sulphidizing, the specimens were submitted to two kinds of heat treatments:

1. Annealing for 18 h at 1150° C, followed by a "intergranular corrosion densensitization" treatment, for 16 h at 700° C. The specimens having undergone this treatment will be described as "desensitized specimens". The grain size is large (200 ~ 300 μm) in both materials. The grain boundaries of the "pure" alloy are practically free from precipitation and some rare bulk chromium oxicarbides are observed (Fig. 3). In industrial alloys a continuous intergranular carbide precipitation is observed, together with a gradient of microcarbides from each side of the grain boundaries.

This heat treatment is reported [16] to induce an equilibrium segregation of phosphorus in the industrial alloy. Some bulk $Cr_{23}C_6$ or $Cr_2(C, N)$ precipitates are also evidenced [7].

2. A recrystallization treatment of 72 h at 800° C is applied to specimens previously "desensitized", and cold-rolled by 60%. In synthetic alloys, the resulting average grain diameter is 20 ~ 30 μm. In industrial alloys, a superimposed network of "ghost" boundaries remaining from the precipitation of the precious desensitized structure, appears (Fig. 4, arrows). The boundaries of the new small grains (20 μm diameter) are free from precipitation.

The subsequent heat treatments, for instance ^{35}S diffusion anneals, can modify those initial microstructures. For desensitized industrial alloys a globularization of the grain-boundary precipitates is essentially to be expected at or beyond 700° C. For recrystallized specimens, grain growth appears for temperature higher than 800° C.

TABLE I Chemical composition of impure alloys

C	Si	Mn	S	P	Cr	Ni	Co	Ti	Cu	Al	Fe
0.072	0.32	0.78	0.003	0.009	16.20	73.65	0.04	0.19	< 0.01	0.11	8.47

TABLE II Calculated evolution of $[V'''_{Cr}]$ or $[V''_{Ni}]$ as a function of pH_2S for Cr_2O_3 or NiO

State of sulphur in the oxide	$Cr_{Cr} = Cr_i^{3+} + V'''Cr + h$ or $Ni_{Ni} = Ni^{+} + V''Ni + h$	$^{3/2}O_2 = 3O_2 + 2V'''Cr + 6h$ or $^{1/2}O_2 = V''Ni + O_o + 2h$
Sulphur on an amionic site in a S_0^- state	$Cr_2O_3[V'''Cr] = \left(\frac{p_{(S_2)}}{p_{(O_2)}}\right)^{1/6} k_1$	$Cr_2O_3[V'''Cr] = \frac{(p_{(S_2)})^{3/8}}{(p_{(O_2)})^{3/16}} k'_1$
	$NiO[V''Ni] = \left(\frac{p_{(S_2)}}{p_{(O_2)}}\right)^{1/6} \times k_1 + k_2$	$NiO[V''Ni] = \frac{p_{(S_2)}}{(p_{(O_2)})^{3/2}} \times k'_1 + k'_2 p_{O_2}^{-1/2}$
Sulphur on a cationic site in a $S^{2+}Cr$ state	$Cr_2O_3[V'''Cr] = (p_{(S_2)})^{1/2} k_3$ or $[V'''Cr] = (p_{(S_2)})^{1/3} k_4$	$Cr_2O_3[V'''Cr] = p_{(S_2)}^{-3/2} \times p_{O_2}^{-3/2} \times k'_3$ or $[V'''Cr] = p_{(S_2)}^{-3/4} \times p_{(O_2)}^{-3/8} \times k'_4$
	$NiO[V''Ni] = \text{constant}$	$NiO[V''Ni] = \frac{(p_{(O_2)})^{1/2}}{(p_{(S_2)})^{1/2}} \times k'_3$
Sulphur on an interstitial site in a Si^- state	$Cr_2O_3[V'''Cr]^2(^3[V'''Cr] + [^9[V'''Cr]^2 + 4(p_{(S_2)}k_5)^{1/2}]^{1/2}]^{1/2} = k_5$	$Cr_2O_3[V'''Cr]^2(^3[V'''Cr] + [^9[V'''Cr] + 4(p_{(S_2)}k'_5)^{1/2}]^{1/2}]^{1/2} = p_{(O_2)}^{3/2} k'_6$
	$NiO\frac{k_6 - [V''Ni]^3}{[V''Ni]^4} = (p_{(S_2)})^{1/2} \times k_7$	$NiO[V''Ni] = \frac{(p_{(O_2)})^{1/2}}{(p_{(S_2)})^{1/2}} \times k'_7$
Sulphur on an interstitial site in a Si^+ state	$Cr_2O_3[V'''Cr] = [1 + (p_{(S_2)}k_8)^{1/2}]^{1/3} k_9$	$Cr_2O_3[V'''Cr] = [1 + (p_{(S_2)}k'_8)^{1/2}]^{1/8} \times p_{(O_2)}^{3/16} k'_9$
	$NiO[V''Ni] = (p_{(S_2)})^{1/4} \times k_{10}$	$NiO2[V''Ni]^{3/2} + \frac{[V''Ni]}{p_{(O_2)}^{1/2}} \times k'_{10} = k'_{11} \frac{(p_{(S_2)})^{1/2}}{(p_{(O_2)})^{-1/4}}$

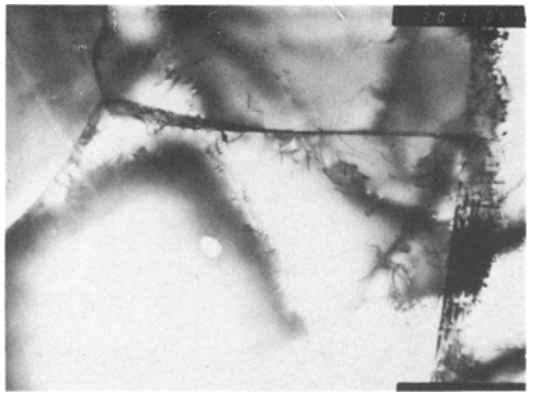

Figure 3 Microstructure of synthetic alloy after desensitizing treatment at 700° C.

3. Fixation and penetration of atomic sulphur

We shall consider here not only the stage of fixation and penetration of atomic sulphur in the surface and in the pre-existing Cr_2O_3 film, but also the penetration of sulphur in an elementary form in the bulk of the material up to distances as large as $200 \simeq 300\,\mu m$ (after 5 h sulphidation at 700° C, under $p(H_2S) = 10^{-4}$ atm).

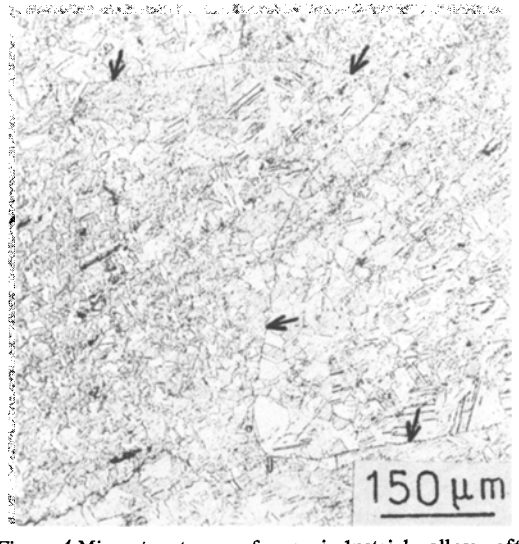

Figure 4 Microstructure of an industrial alloy after recrystallizing treatment at 800° C (note the ghost of first desensitizing grain boundaries shown by the arrows).

3.1. Sulphur in the oxide surface Cr_2O_3 film

3.1.1. Initial stage

The initial stage of the sulphidation kinetics is described by a parabolic law. The constants of the parabolic law, kp, follow the relations:

$$kp = p\,S_2^n \qquad (1)$$

with $n = +1/1.74$ for the industrial alloy (Fig. 5a) and $n = -3/4.8$ for the synthetic alloy (Fig. 5b).

Such laws can be interpreted only if one considers that the diffusing species is S^{2+} through chromium vacancies V_{Cr}''' of the Cr_2O_3 lattice as other authors [17]. In that initial state of sulphidization, the parabolic constant is proportional to the vacancy concentration $[V_{Cr}''']$:

$$kp \propto D \propto \Gamma \times g \times [V_{Cr}'''] \qquad (2)$$

where D is the diffusion coefficient, Γ is the jump frequency and g is the geometrical factor.

A comparison with the possible theoretical laws arising from different vacancy formation processes (Table II) leads us to propose the following mechanisms* [9]:

for industrial alloys:

$$Cr_{Cr} = V_{Cr}''' + Cr_i^{2+} + h^{\cdot} \qquad (3)$$

then

$$[V_{Cr}'''] = k_1\,pS_2^{1/2} \qquad (4)$$

for synthetic alloys:

$$3/2\,O_2 = 3\,O_0 + 2\,V_{Cr}''' + 6\,h^{\cdot} \qquad (5)$$

then

$$[V_{Cr}'''] = k_2 p\,S_2^{-3/4}\,pO_2^{-3/8}. \qquad (6)$$

That analysis is valid only for the shortest sulphidation times when no important variation of the defect concentration or of the ionic form of sulphur is observed. A variation of the defect concentration may, in particular, be induced by the presence of doping elements as impurity elements (titanium, silicon) or other constitution elements (as nickel, iron) [19].

The change in vacancy formation and S^{2+} diffusion mechanism from the impurities to the industrial alloys may be explained by the influence of impurities which could modify the vacancy

*The formulation used in defect formation equation is [18]: Cr_{Cr} = chromium atom on a chromium site, V_{Cr}''' = chromium vacancy with 3 charges, Cr^{2+} = interstitial chromium with 2 charges, $h^{\cdot}$ = electron holes, O_0 = oxygen atom on an oxygen site.

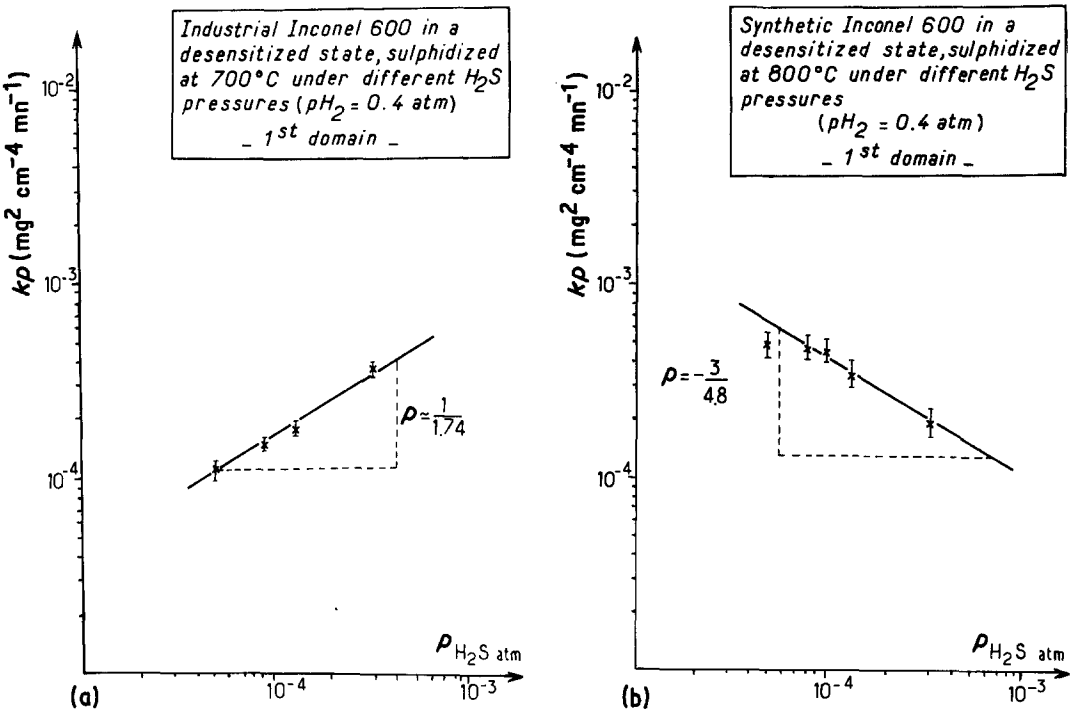

Figure 5 Evolution of kp as a function of $p(H_2S)$ during the first sulphur pollution step for both alloys in a desensitized state.

formation parameters. A complete study on doped Cr_2O_3 massive oxide would be necessary, but it does not exist for the moment.

The activation energy of this first step is high. The experimental values of 600 to 750 kJ mol^{-1} must be considered as only indicative as they include several associated processes: dissociative adsorption, dissolution and diffusion of sulphur in the film. It can be furthermore affected by other chemical reactions.

Among all the processes associated with this activation energy, the sulphur dissolution is the most difficult to estimate. The dissolution of sulphur as S^{2+} ions in chromium atom sites can be described by the following equation:

$$1/2\ S_2^{2-}\ \text{ads} \rightleftarrows S_{Cr}^{2\pm} + 2/3\ V_O^{\cdot\cdot} + 2/3\ e \qquad (7)$$

($S_{Cr}^{2\pm} = S^{2+}$ on a chromium atom site, with a negative charge with respect to the lattice, $V_O^{\cdot\cdot}$ = oxygen vacancy with a double positive charge). Nevertheless such a mechanism is not clear.

3.1.2. Stage of competition between reduction and sulphidation

Beyond 3 to 5 h in H_2/H_2S atmosphere, the first-order reaction of reduction of Cr_2O_3 becomes predominant especially in synthetic alloys (Table III) as shown by the quasi-linear dependence of the constant kp to $p(S_2)$.

Simultaneously, one observes the formation, in the sulphidizing device, of H_2O trapped on the native copper of the Cu_2S furnace, a large dissolution (up to 10 wt%) of sulphur in the surface film (Figs. 6a and b), and a small activation energy for the process (112 kJ mol^{-1}), even smaller than the calculated Cr_2O_3 reduction energy (280 kJ mol^{-1} at 700° C) [11] (Table IV). These results are in agreement with a process of substitution of O^{2-} by S^{2-} in the surface of Cr_2O_3 film.

3.2. Sulphur penetration into the bulk alloy

The penetration of sulphur into the underlying alloy is nearly instantaneous (Fig. 7). It is then necessary to acquire data on atomic sulphur diffusion phenomena in these alloys. Sulphur dissolves in metals (iron, nickel, copper, silver) substitutionally [20, 21]; it has been reported to be preferentially located at grain boundaries, which means that the sulphur-defect interaction is large [22]. Both quantitative diffusion measurements of ^{35}S and high resolution autoradiographic observations of ^{35}S spatial distribution have been performed.

TABLE III Evolution of kp as a function of pH_2S for the different H_2S pollution steps

		Synthetic alloy	Industrial Alloy
Competition between Cr_{2O3} reduction and CrS formation		$3 < t < 20$ h $kp \propto p(H_2S)^{1,2}$	$3 < t < 16$ h $kp \propto p(H_2S)^{1/6,4}$
Growing of sulphide (S)-layer (S)	1st state	t_0 70 h $kp \propto p(H_2S)^{1/6}$	t_0 70 h $kp \propto p(H_2S)^{1,1}$
	2nd state	t_0 100 h $kp \propto p(H_2S)^{1,2}$	t_0 100 h $kp \propto p(H_2S)^{1/4,8}$

3.2.1. Diffusion parameters [6]

The bulk sulphur diffusion coefficients follow an Arrhenius law, with an activation energy $Q_v = 217 \pm 1$ kJ mol^{-1} and a frequency factor $D_0 = 0.1$ to 1 cm^2 sec^{-1}).

This activation energy is smaller than the energy for nickel self-diffusion (275 kJ mol^{-1}) [23] and the sulphur D_v values are 10 times larger in these alloys than in pure nickel [24]. This proves that a single vacancy mechanism seems to be excluded and that sulphur-impurity interactions must be taken into account; recent results [25] have shown that sulphur–sulphur interactions would be negligible.

The grain boundary diffusion parameters $D_j\delta\alpha$ (D_j is the grain boundary diffusion coefficient, δ is the grain boundary thickness and α is the segregation rate of sulphur in the grain boundaries) are shown in Fig. 8. The average activation energies are: -110 kJ mol^{-1} in the industrial "desensitized" alloy, -253 kJ mol^{-1} in the industrial "recrystallized" alloy, -213 kJ mol^{-1} in the synthetic "densensitized" alloy, -320 kJ mol^{-1} in the synthetic "recrystallized" alloy.

A large drop of the $D_j\delta\alpha$ values occurs about 950° C and has been attributed to the redissolution of carbides occurring during the diffusion anneal itself (see next section).

The difference in activation energies between industrial alloys and synthetic alloys is due to the role of impurity precipitations (specially chromium carbides) on grain boundary diffusion. The role of

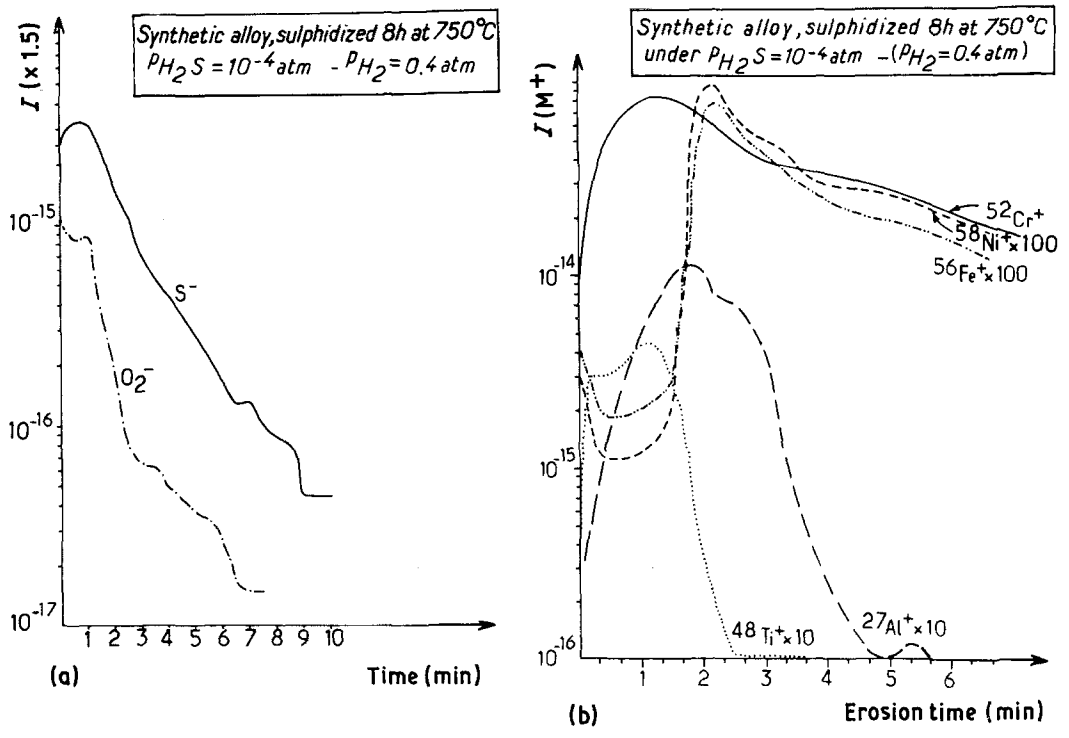

Figure 6 SIMS analysis of the Cr^+, Ni^+, Fe^+, Ti^+, Al^+, S^-, O_2^- evolution through the external Cr_2O_3 layer as a function of the erosion time. (Synthetic alloy in a desensitized state, then sulphidized under p (H_2S) = 10^{-4} atm at 750° C).

TABLE IV Activation energies for the H_2S pollution process during the different sulphidizing states. (Synthetic and industrial alloys in a desensitized state, then sulphidized at 700° C under $pH_2S = 10^{-4}$ atm.)

Domain		Energy (kJ mol^{-1})	
		Synthetic	Industrial
Competition between Cr_2O_3 reduction and CrS formation		112.6	290.8
Growing of sulphide (S) layer(s)	1st state	349.6	330.4
	2nd state	133.6	39.3

the high-dislocation density in the vicinity of the carbides has also to be taken into account [6].

3.2.2. Microstructural location of ^{35}S, by HPR autoradiography

After diffusion annealing, the atomic radioactive sulphur is essentially located, when no other defects are present, along the grain boundaries (Fig. 9). In the bulk of the grains, some silver grains of the autoradiography are observed on the twin boundaries (Fig. 10).

When dislocations are present, the sulphur distribution is modified by the sulphur–dislocation interactions. The result of this can be a certain spreading of sulphur on each side of the grain boundaries (Fig. 11). Precipitates and dislocations in their vicinity are strong trapping sites for sulphur (Fig. 12). In a "recrystallized" specimen this effect can even lead to a higher ^{35}S concentration in the matrix than in the grain boundaries (Fig. 13).

In the temperature range 900 ~ 1000° C when chromium carbide dissolution occurs during the diffusion anneal, the strong carbon–sulphur or chromium–sulphur interaction results in a random spreading of ^{35}S from the grain boundaries into the volume (Fig. 14). This is the explanation of the previously mentioned drop of the $D_j\delta\alpha$ [6].

3.3. Discussion on the atomic sulphur pollution stage

In the pre-existing Cr_2O_3 layer, all kinds of sulphur transport phenomena are favoured by a factor of 10^2 to 10^3 as compared to chromium diffusion phenomena. From the observed influence of all kinds of defects, one has to consider not only a distinct analysis of atomic sulphur attack processes in the surface oxide layer and in the bulk alloy, but also a differentiation of the mechanisms linked with metallurgical parameters such as purity and microstructures.

Considering now the diffusion measurement results, they can be interpreted as a first approximation and for synthetic alloys, by a dislocation-assisted general diffusion mechanism, as already observed for other fcc alloys [26]. The interpretation is supported by the comparison of the activation energies for diffusion and vacancy formation energies and by the observation of preferential sulphur–dislocation interaction.

But this analysis is not rigorous for industrial alloys in which the diffusion paths are modified, for instance by the presence of chromium carbides and associated high dislocation densities. The latter seem to act as diffusion short-circuit.

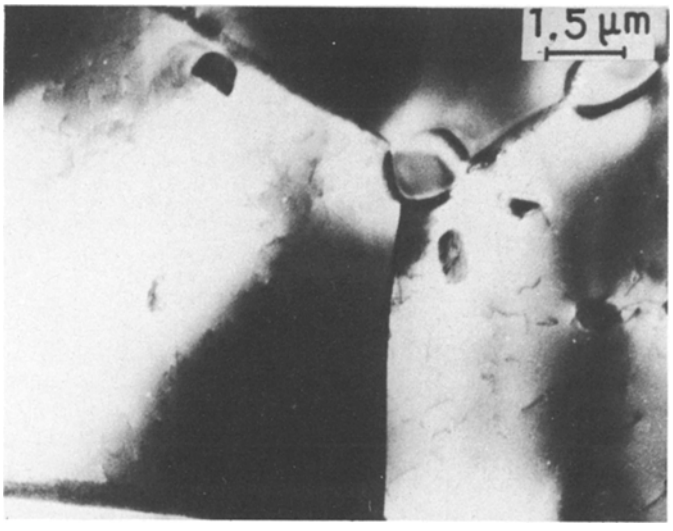

Figure 7 Instantaneous microsulphide nucleation after 8 h of H_2S pollution process at 700° C. (Industrial alloy in a previous desensitized state.)

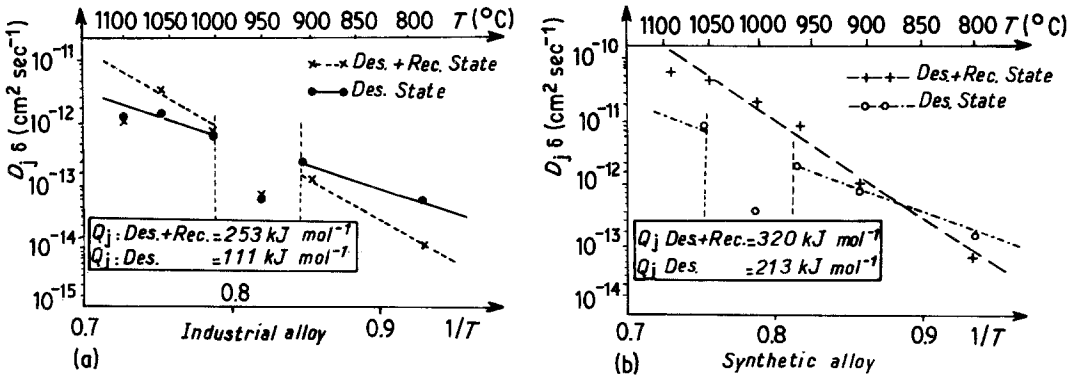

Figure 8 Evolution of the intergranular diffusion parameter of sulphur ($D_j\delta\alpha$) as a function of $1/T$, for both the alloys in a desensitized or recrystallized state.

4. Atomic sulphur gathering as clusters or 2D compounds

This stage of the sulphur pollution is very rapid and is rarely accounted for in usual sulphidation studies. The interest of the low H_2S pressure experiments performed here (equivalent $p(S_2)$ from 10^{-14} to 10^{-12} atm) then appears clearly. Such a stage can be defined as the period when a full competition appears between the pure diffusional processes and the thermochemically controlled reactions. This is true on the surface as well as inside the volume of the material.

4.1. Surface Cr_2O_3 layer

Thanks to the relative stability of Cr_2O_3 (ΔG of reduction at 800° C = 278 kJ mol^{-1}) one can consider the specific behaviour of sulphur. From the concentration profiles obtained by secondary ion mass spectrometry (SIMS) (Fig. 15) an accumulation of sulphur at the Cr_2O_3/underlying alloy interface is evidenced. This phenomenon may be discussed from both the kinetic and thermodynamical point of view.

4.1.1. Kinetic aspect

The mobility of sulphur in Cr_2O_3 ($D_1 = 10^{-10}$ cm^2 sec^{-1} at 800° C) is 10 times larger than in the alloy ($D_2 = 10^{-11}$ cm^2 sec^{-1} at 800° C) [6, 27]. However, the value mentioned here for D_1 was obtained [26] with a very fine grain (3 μm) oxide, which is not the case here and this grain size factor may be very large, as noticed by Wagner [27]. Furthermore, the composition of the Cr_2O_3 layer may vary towards a sulphur-enriched (up to 10 wt %) oxide and this can also be a factor in diffusion enhancement. Simultaneously, the thickness of the Cr_2O_3 film decreases (from 3 to 1.5 μm in 24 h for instance).

Chromium diffusion from the bulk to the surface also takes place during the process, directly evidenced by SIMS profile measurements and microprobe analysis in the underlying alloy.

The empirical kinetic laws of chromium depletion are: $\Delta\%Cr \propto t^{-1/5}$ for the synthetic alloy (Fig. 16a) and $\Delta\%Cr \propto \exp(0.01\ t)$ for the industrial alloy (Fig. 16b). But as the chromium diffusivities are equivalent in the metal and in the oxide

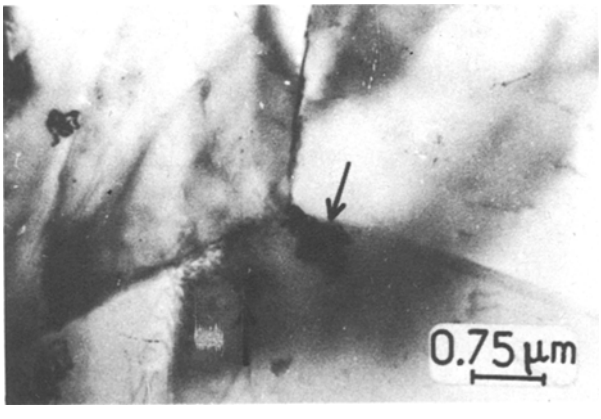

Figure 9 Localization of silver filaments on triple points. Synthetic alloy in a desensitized state after sulphidizing treatment at 650° C. High resolution autoradiography with ^{35}S.

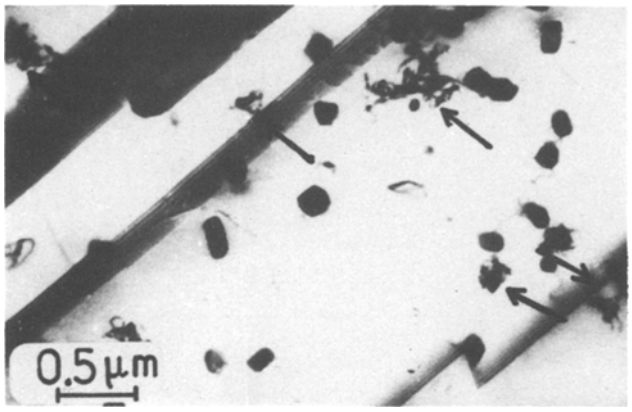

Figure 10 High resolution sulphur autoradiography. Segregation of sulphur on the carbides along the slip planes in a recrystallized industrial alloy. Sulphidizing treatment 4 h at 800° C.

[28, 29], it appears that neither sulphur diffusion argument nor chromium diffusion argument are sufficient to explain the sulphur accumulation at the Cr_2O_3/metal interface.

4.1.2. Thermochemical aspect

The first factor to be considered is the interaction between sulphur and the alloy elements. Interaction studies in multicomponent systems (ternary systems) [30] usually consider interaction parameters.

$$\alpha'_{M,I} = \alpha'_{M,I} - \alpha'_{MM}. \quad (8)$$

Where α and α' binary interaction coefficients among the two metals (M, M') and the impurity (I). By analysing the situation for the system (chromium, sulphur, nickel) and (iron, sulphur, nickel), one finds that:

$$\alpha'_{CrS}\,(224\,\text{kJ mol}^{-1}) \gg \alpha'_{FeS}\,(12.5\,\text{kJ mol}^{-1})$$

(Table V). (9)

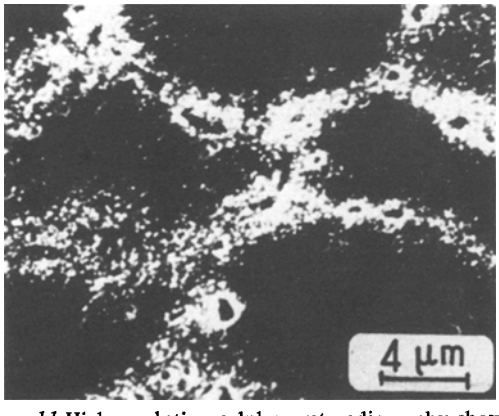

Figure 11 High resolution sulphur autoradiography showing a spreading of sulphur on each side of the grain boundaries. Recrystallized synthetic alloy after a sulphidizing treatment 4 h at 800° C.

A second factor is the possible lowering of the oxide/interface energy: a sulphur monolayer ($\simeq 7.4 \times 10^{-14}$ atm cm^{-2}) may induce an important interface energy drop, according to the Gibbs adsorption analysis. The experimental activation energies measured at this stage of the pollution process (Table IV) are different from the segregation energies. Moreover the constant of sulphidation, kp, versus $p(S_2)$ curve (Table III) is of a first-order reaction type. Thus this stage may be in fact controlled either by a sulphur substitution in the Cr_2O_3 layer on the synthetic alloy ($Q \simeq 112$ kJ mol^{-1}), or by reduction of the Cr_2O_3 layer on the industrial alloy ($Q \simeq 290$ kJ mol^{-1}).

4.2. Underlying alloy

4.2.1. Morphological and analytical aspect

At this stage, most of the sulphur clustering process occurs on the grain boundaries, which are the best accomodation sites. The "Baumann microprint" observations, showing a continuous distribution of Ag_2S spheres along the grain boundaries (Fig. 17), indicate the presence of a continuous sulphide layer in the boundaries. The purity of the grain boundaries is the most important parameter. In impurity-free boundaries in "desensitized" synthetic alloy, a strong sulphur collection occurs, as shown by Auger spectrometry (Fig. 18). The contents of the alloying elements are not much modified, except for a sensible chromium depletion which may be due to the desensitization treatment itself. This behaviour is observed even after very long times (100 h sulphidization anneals at 800° C under very low H_2S pressure).

When the grain boundaries are polluted with other impurities (phosphorous equilibrium segregation, chromium carbide precipitation), the

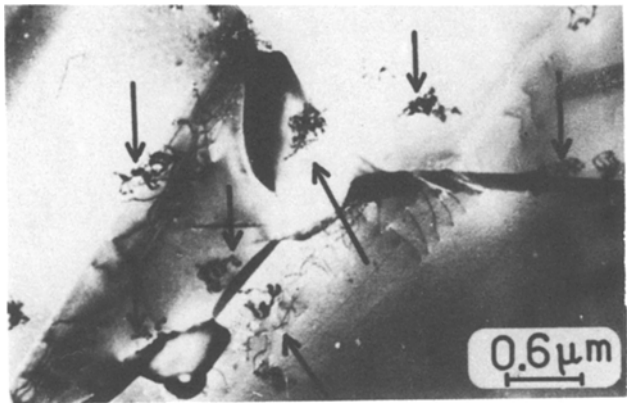

Figure 12 Silver filaments which segregated in a preferential way on the dislocations near the intergranular carbides of a recrystallized industrial alloy at 800° C–^{35}S HPR autoradiography.

kinetics of sulphur [16] gathering is altered. No sensible grain boundary sulphur accumulation is observed by Auger electron spectroscopy (AES) after 25 h sulphidation ($p(H_2S) = 10^{-4}$ atm) (Fig. 19). Meanwhile, the phosphorous segregation is still visible. Incidentally, one can notice an accumulation of boron.

In order to try to discriminate the relative effects of segregated phosphorous and of carbides, the following two experimental results must be mentioned:

1. Firstly, the overall grain boundary amount of sulphur, after given sulphidization conditions, is larger in impure (carbide-containing) grain boundaries than in pure boundaries (Fig. 17).

2. Secondly, sulphur accumulations in industrial alloys occur more densely on transgranular carbides than on grain boundaries (Fig. 12).

Thus, the whole process can be explained by a competition between sulphur and phosphorous segregations, resulting in a slowering of the former by the later. This effect has been reported in the literature for surface segregations of phosphorous at 700° C and sulphur at 800° C on the same alloy [31].

4.2.2. Thermodynamical aspect

The phenomenon is not really an equilibrium segregation process [32]. An estimation of sulphur solubility can be done through the Hillert's analysis of equilibrium solubility [33].

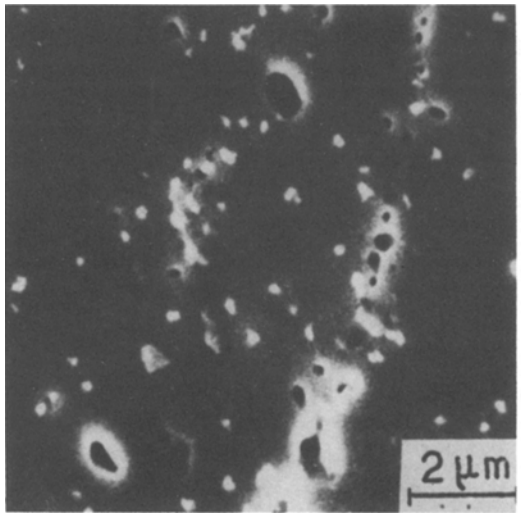

Figure 13 Distribution of silver filaments in the matrix of industrial alloy in a previous recrystallized state and after diffusion treatment at 800° C. (Scanning electron observation of ^{35}S autoradiography).

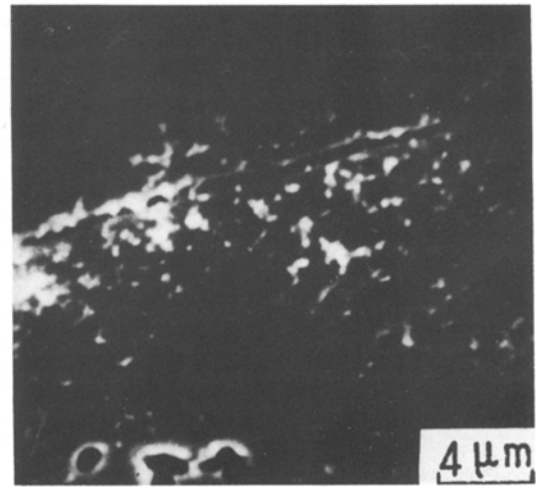

Figure 14 Random distribution of sulphur ^{35}S (or silver filaments) from the grain boundary of an industrial alloy in a previous desensitized form, after a sulphur diffusion treatment at 950° C.

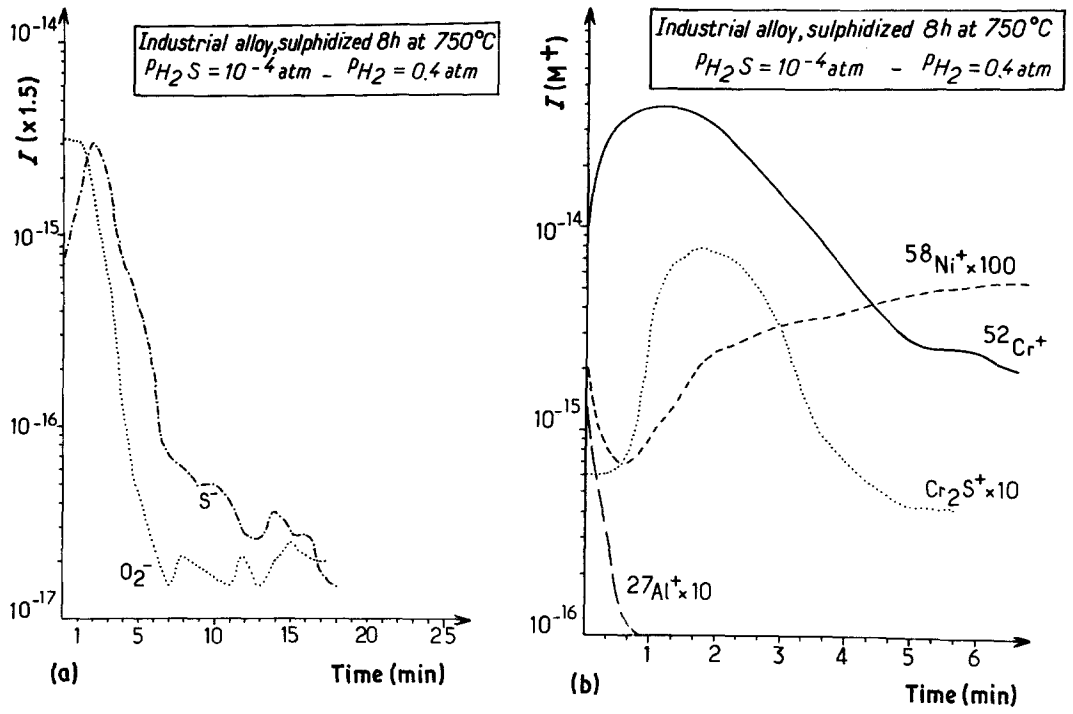

Figure 15 SIMS analysis of the Cr^+, Ni^+, Cr_2S^+, Al^+, S^- and O_2^- evolution through the external Cr_2O_3 layer as a function of the erosion time. (Industrial alloy in a desensitized state, then sulphidized under $p(H_2S) = 10^{-4}$ atm at 750° C.)

$$C_S = C'_S \left\{ 1 + \left[\exp\left(\frac{\beta_{MS}}{aRT} \right) - 1 \right] C_M \right\}^{-a/c} \quad (10)$$

where C_S is the sulphur solubility in ternary Cr–Ni–S alloy, C'_S is the sulphur solubility in ternary CrS alloy, β_{MS} is the bulk Cr–S or Ni–S interaction coefficient [33]. $a/c = 1$ for Ni–S and Cr–S and M = Cr or Ni. The estimated value solubility is extremely low ($\simeq 10^{-5}$) and not in agreement with experiment. The system is thus out of equilibrium and this is illustrated by the existence of a chromium flux toward the surface (Fig. 16).

4.2.3. Structural aspect

The nature of the bounds which lead to the formation of the intergranular sulphur layer cannot be established directly. The most recent models for grain boundary embrittlement account for the existence of S–S covalent [34] or M–S (with M = Ni or Cr) heteropolar [35] bounding leading to a weakening of the M–M bounds.

Experimentally, an indication is given by the response to the "Baumann microprint" test: it has been established that the sensitivity threshold of this test is the presence of a two-dimensional intergranular compound [15]. A positive answer of this "Baumann microprint" then, leads to conclude of the existence of a two-dimensional compound with specific S–S or M–S bounds.

Another indication is the absence of measurable alloying element enrichment on the grain boundaries (Fig. 18), which rules out the hypothesis of a Cr–S two-dimensional compound. This confirms the validity of a Loesch model [34]: as the S–S bounding energy (265 kJ mol^{-1}) is larger than the P–P bonding energy (215 kJ mol^{-1}), sulphur should then be a stronger embrittlement than phosphorous. This is indeed the experimental result obtained (Fig. 20).

5. Chromium sulphide nucleation

During that stage, the role of grain boundaries and all other microstructural defects (as chromium carbide) is emphasized.

5.1. Surface layer

The free enthalpy ΔG for microsulphide nuclei formation can be calculated, for instance by considering the nuclei as flattened spheroids of equatorial radius a and polar radius c [36]:

$$\Delta G = \tfrac{4}{3}\pi a^2 c \Delta G_v + 2\pi a^2 \gamma \quad (11)$$

where ΔG is the volume free enthalpy of sulphide formation and γ = sulphide/alloy interface energy.

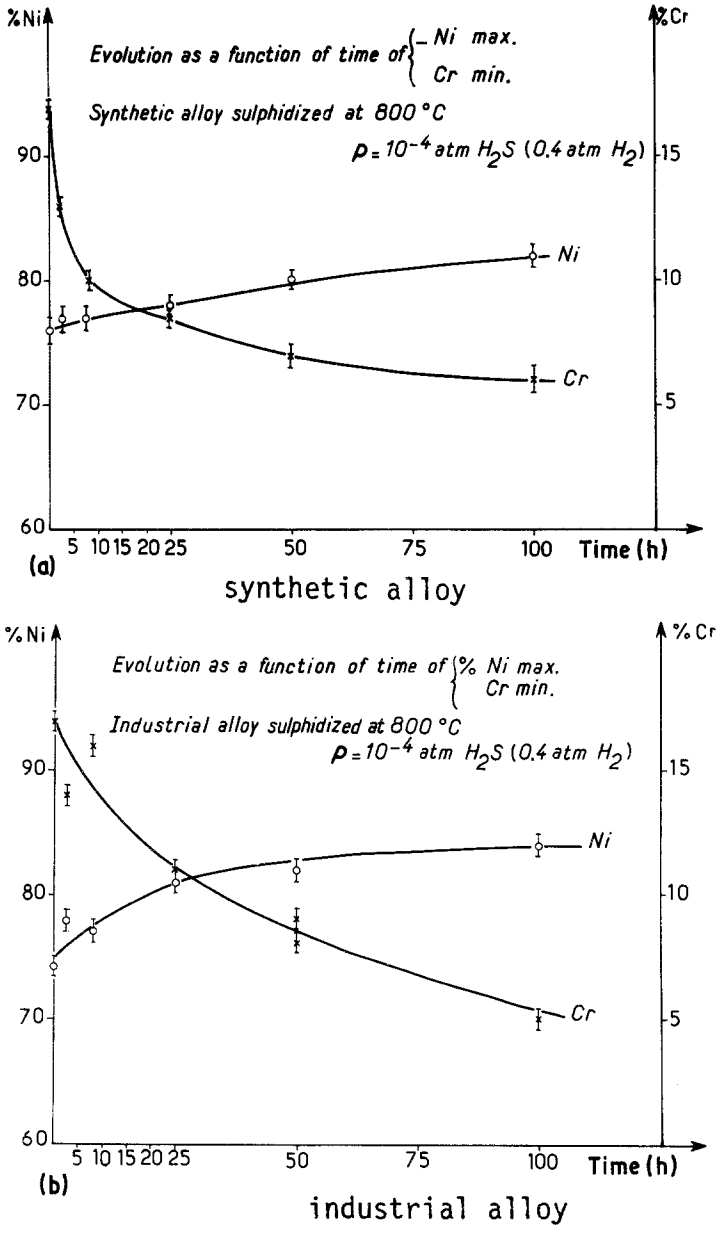

Figure 16 Evolution of the nickel and chromium percentage in the external Cr_2O_3 underlying alloy in a previous desensitized state, then sulphidized at 800° C under $p(H_2S) = 10^{-4}$ atm.

Starting from literature data [37, 38], one can calculate the critical $p(H_2S)p(H_2)$ value for sulphide nucleation (Table VI). The calculated values are in good agreement with experimental values and explain the sequence of formation of sulphides observed as a function of temperature or $p(H_2S)$ [5].

$$\Delta G_{TiS} > \Delta G_{Al_2S_3} > \Delta G_{CrS} > \Delta Cr_3S_4 > \Delta G_{FeS} > \Delta G_{Ni3}S_2 > \Delta G_{NiS_2}. \quad (12)$$

TABLE V Standard enthalpies of CrS and NiS formation, ΔH^0, and relative interaction coefficients α' between Cr and S in the (Cr, S, Ni) system and between Fe and S in the (F, S, Ni) system.

System	Thermodynamic data (kJ mol^{-1})		
	ΔH^0	α	α'
Cr, S, Ni	NiS = 146.3 CrS = 202.3	NiS = 585.2 CrS = 809.3	CrS = 224
Fe, S, Ni	FeS = 149.4	FeS = 597.7	FeS = 12.5

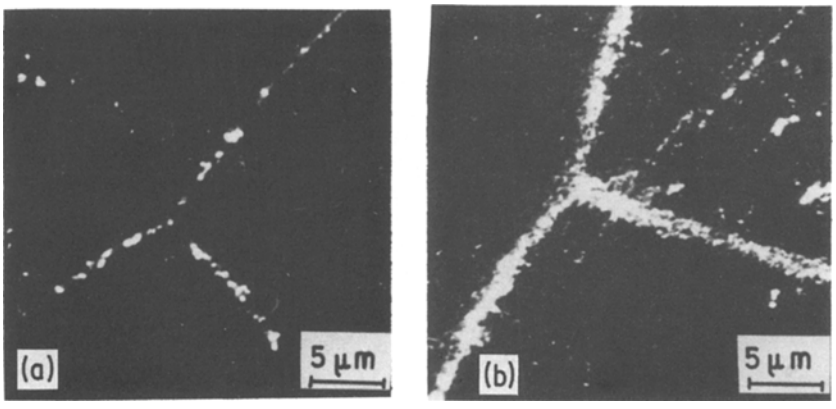

Figure 17 Baumann microprint test showing a continuous Ag_2S spheres collection along the grain boundaries. Alloys in a desensitized state, then sulphidized 8 h at 700° C under $p(H_2S) = 10^{-4}$ atm.

It must be noted that the calculations do not take into account a possible reduction or sulphur substitution in Cr_2O_3.

These results explain also the observed shift of the surface chromium sulphide nucleation times toward shorter times (8 h under $p(H_2S) = 10^{-4}$ atm) in the case of industrial alloy: the existence of chromium-rich precipitates near the surface increases the chromium activity.

5.2. Bulk attack

Microsulphide nucleation is favoured on the grain boundaries and on the pre-existing chromium carbides (Fig. 21).

5.2.1. Crystallographic aspect

Most of chromium sulphides are hexagonal. It has been verified that the microsulphides are incoherent with respect to the matrix except in one single case (pure "recrystallized" alloy, sulphidized 30 h at 800° C under 10^{-4} atm H_2S).

5.2.2. Thermodynamical aspect

The first problem is to evaluate the interface energy, γ_F, of the nuclei. The well known Lifshitz–Wagner analysis [39] leads to:

$$\gamma_F = 9/8 \frac{RT(r^3 - r_0^3)}{CeV_m^2 D(t - t_0)} \qquad (12)$$

where r (r_0) are the average precipitate radii at times t (t_0), D is the chromium diffusion coefficient, and V_m is the molar volume of the sulphide (21.6 cm^3 mol^{-1}).

The values obtained (Table VIII) are of course very roughly estimated as the chromium bulk diffusion growth process is only valid for matrix

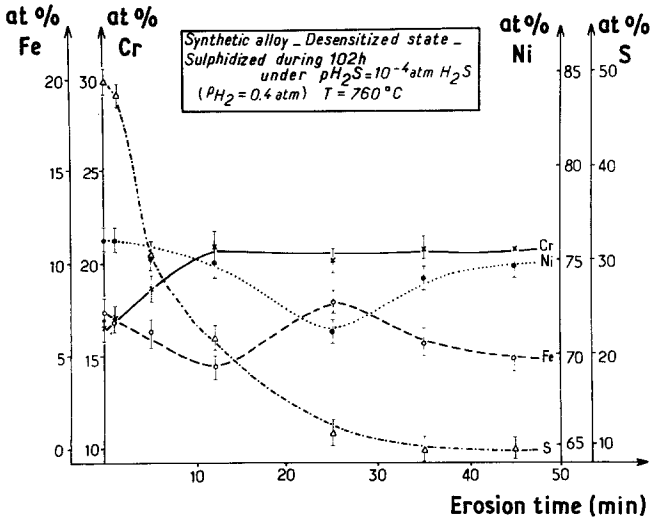

Figure 18 Auger spectrometry analysis of the Cr, Ni, Fe, S evolution in the two or three layers near the grain boundary of synthetic alloy in a desensitized state, then sulphidized 102 h at 760° C, under $p(H_2S) = 10^{-4}$ atm.

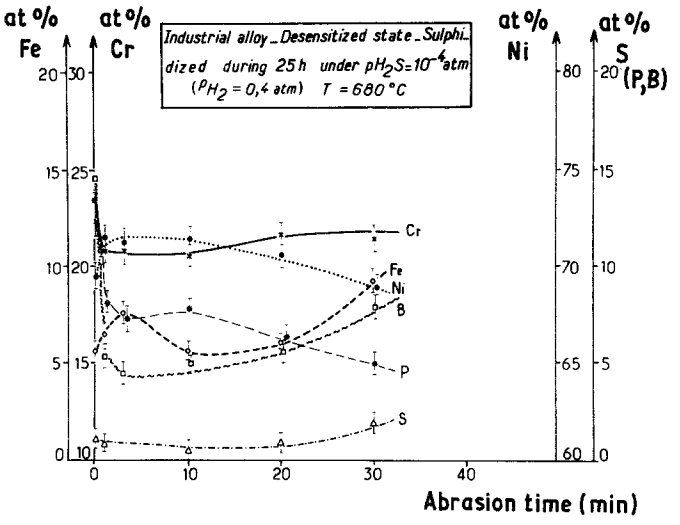

Figure 19 Auger spectrometry analysis of the Cr, Ni, Fe, S, P, B evolution in the 2 or 3 layers near the grain boundary of industrial alloy in a desensitized state, then sulphidized 25 h at 680° C, under $p(H_2S) = 10^{-4}$ atm.

sulphides of "desensitized" synthetic alloys (where $r \propto t^{1/3}$ is actually observed). In grain boundaries the diffusion process is evidently modified; in industrial alloys, chromium is not the only diffusing species; generally the sulphides are in fact of complex composition (Table VII). Moreover, lack of stoichiometry can even be observed. The very high values of Table VIII must then be considered as only indicative of comparative trends. One may then try to estimate the critical energies for sulphide nucleation. The analysis by Burke [36] gives:

$$W^* = \frac{8}{3} \frac{\pi^3 \mu^2 \Delta^4 \gamma_F^3}{(\Delta G_v)^4} \qquad (13)$$

where μ is the matrix elastic shear modulus, and Δ is the expansion coefficient between the matrix and the precipitates (e.g. $\Delta = 3.9$ for $Cr \rightarrow Cr_2S_3$ [40]. For Cr–S, $\Delta G_V = 1795 - 13.24\,T$ kJ mol^{-1} [37, 38].

The critical values obtained are given in Table IX. It is clear that such values are not realistic, although already mentioned for other systems [41], specially for low temperatures, but it is not clear that the calculation is affected by the poor accuracy of γ_F estimation. The results should nevertheless be considered as an indication of a large variation of W^* with temperature and as a proof that, at low temperature, another mechanism of nucleation is acting. Discontinuous nucleation on microstructural defects (slip planes, dislocations, twin planes, grain boundaries) becomes the controlling process, even on synthetic alloys.

In industrial alloys, the preferential sulphide

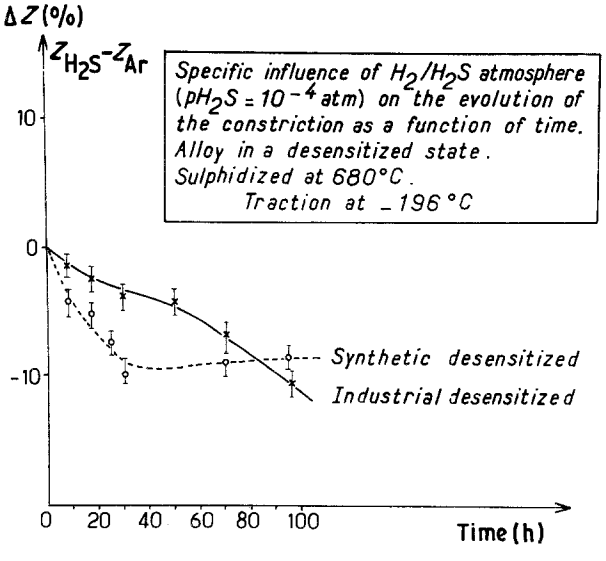

Figure 20 Reduction of area as a function of the H_2/H_2S sulphidizing treatment time. Synthetic and industrial alloys in a desensitized state, then sulphidized at 680° C under $p(H_2S) = 10^{-4}$ atm.

TABLE VI Ratios of critical pressures $p(H_2S)/p(H_2S)$ for the formation of 650° C of the different external sulphidized phases for pure metals or $Ni_{77}Cr_{66}Fe_7$ alloy

Critical $P(H_2S)/P(H_2)$ for sulphide formation	CrS	Ni_3S_2	FeS	TiS_2
Pure metals	1×10^{-6}	3×10^{-3}	6×10^{-3}	15×10^{-6}
Inconel 600 calculated	6×10^{-6}	5×10^{-3}	9×10^{-3}	2×10^{-5}
Inconel 600 experimental	$(2.5) \times 10^{-5}$	$(2-4) \times 10^{-2}$	$(2-4) \times 10^{-2}$	10^{-5}

TABLE VII Evolution of the external sulphidized phases composition as a function of the sulphidizing temperature or of the microstructural state. Inconel 600 sulfidization 100 h under $p(H_2S) \simeq 10^{-4}$ atm

Temperature (° C)	Microstructural state	
	Desensitized state	Recrystallized state
< 900° C	$(Cr_{0.91}Ni_{0.07}Ti(Al)_{0.02})_7S_8$	$(Cr_{0.89}Ni_{0.05}Ti(Al)_{0.06})_3S_4$
≃ 1000° C	$(Cr_{0.89}Ti_{0.1}Ni_{0.01})_7S_8$	Synthetic alloy
	Possibly	$(Cr_{0.97}Ni_{0.02}Ti_{0.01})S$
	$(Cr_{0.89}Ti_{0.1}Ni_{0.01})S$	Industrial alloy
		$(Cr_{0.97}Ni_{0.02}Ti_{0.01})_7S_8$

nucleation on $Cr_{23}C_6$ carbides is a consequence, as already mentioned, of:

1. The higher chromium activity around the carbides.

2. The energy gain associated to the formation of CrS from $Cr_{23}C_6$ instead of solid solution (this is not true for oxides).

3. The importance of the "overcrowding factor", Δ, which is for instance decreased to $\Delta_2 = 8.3 \times 10^{-2}$ for the formation of Cr_3S_2 from $Cr_{23}C_6$, instead of $\Delta_1 = 3.9$ for the formation of Cr_3S_2 from the solution solution; thus $(\Delta_2/\Delta_1)^4 \simeq 10^{-7}$.

In such a process the sulphide growth is not hindered by the carbide dissolution as the diffusion coefficient of carbon is 100 times larger than the sulphur diffusion coefficient.

6. Growth of the external and internal sulphidized layers

This stage is controlled by the multicomponent diffusion phenomena: chromium and sulphur diffusion and also diffusion of impurities (carbon, oxygen, metallic impurities).

6.1. Surface sulphidation

The growth of the facetted layer (Fig. 22) follows a parabolic kinetic law (Fig. 23).

6.1.1. Quantitative and analytical study

The variation of the parabolic constants *kp* obtained from experimental curves as a function of the sulphur pressure have been reported in Table III. The sulphur layer growth stage must again be divided, from this point of view, in two successive steps.

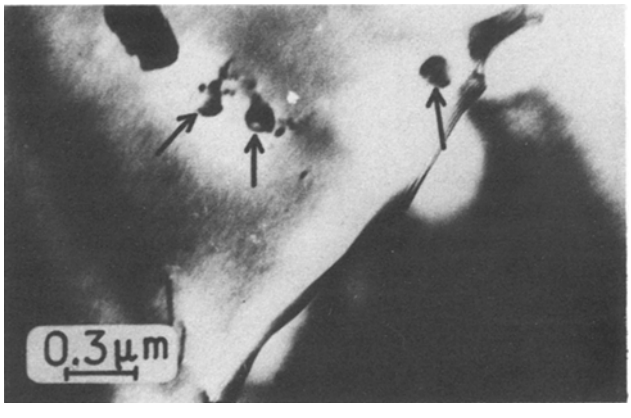

Figure 21 High-resolution sulphur microprint Ag_2S spheres are located on the dislocations near the carbides. Industrial alloy in a desensitized form, sulphidized for 4 h at 800° C.

TABLE VIII Calculated interfacial energies, γ, as a function of temperature

Interfacial energy	Temperature (°C)			
	650	800	900	1000
γ ($\times 10^{-5}$ J cm^{-2})	125	30.00	9.00	2.50

It is clear that this analysis is valid only if the variation of $p(H_2S)$ do not infere a basic change in the layer composition. This is why these laws have been obtained for somewhat narrow H_2S (or equivalent S_2) pressure domain ($10^{-14} \leqslant p(S_2) < 10^{-12}$ atm).

From Table III, the pressure dependence laws can be divided into two families:

1. Quasilinear laws (exponent close to 1.1 or 1.2) indicating a first-order reaction, which could be a "chemical reaction" (Cr_2O_3 reduction, for instance), or a gas diffusion law through a porous layer.

2. $p(H_2S)$ laws, with $1/6.4 < n < 1/4.8$, which are similar to growth laws observed in usual oxidation phenomena in the case of p semiconductor oxides [42].

The activation energies for the different stages are given in Table IV.

The results of the analytical phase identification [5] are summarized in Fig. 24 for the different sulphidation steps. It can be seen that the presently described stage is essentially controlled by the growth of a chromium sulphide layer underneath the chromium oxide, except for the last step of sulphidation of the synthetic alloy. In this last case a layer of impurity sulphide (sulphide containing titanium, aluminium and chromium) appears at the metal/chromium sulphide interface for the long sulphidation durations; the $p^n_{(H_2S)}$ law is then quasilinear and the reaction is probably controlled by gas diffusion through the porous chromium sulphide and/or a first order chemical reaction with an activation energy of 134 kJ mol^{-1} (Table IV).

6.1.2. Discussion of diffusion processes

The growth of the chromium sulphide layer (pH_2S law with $1/6.4 < n < 1/4.8$) is obviously controlled by solid-state diffusion. The activation energies are very different for the synthetic (113 kJ mol^{-1}) and the industrial (330 kJ mol^{-1}) alloys. Again, microstructural arguments (presence of high chromium activities near the $Cr_{23}C_6$ carbides, for instance, and part of non-stabilized compound in the matrix like titanium, aluminium, chromium) should be taken into account by a very important parameter is the ratio of the chromium self-diffusion coefficient in the layer (D_1) and in the metal substrate (D_2) following the analysis proposed by Lalauze [43].

We propose the following expressions:

$$\text{if } D_1 \gg D_2, kp = \frac{2D_2N_{Cr}^2}{\pi} \quad (14)$$

$$\text{if } D_1 \ll D_2, kp = AD_1(P_e - P_i) \quad (15)$$

where N_{Cr} is the atomic fraction of chromium in the alloy, P_e is the gas pressure at the external surface of the layer, P_i is the equivalent gas pressure at the internal interface of the layer. The kinetics of chromium depletion (i.e. N_{Cr} variation) in the underlying zone of the two alloys (Fig. 16) and the correlative variations of the diffusion coefficients D_1 and D_2 may then be responsible of the fact that for the same duration, an alloy self-diffusion controlled mechanism (Equation 14) is operative in the synthetic alloy, whereas a pressure-controlled mechanism (Equation 15) is evidenced in the industrial alloy. For very long sulphidation of the synthetic alloy, another diffusion-controlled mechanism appears, probably as a consequence of the extreme depletion of the alloy and of the large thickness of the sulphide scale.

6.2. Internal sulphidation

6.2.1. Sulphide precipitation

The analysis of the thickness x of the internally sulphidized layer shows up again, two different growing kinetic laws:

$x = A_1 t$ for the industrial alloy

("desensitized state")

$x = A_2 t^{0.39}$ for the synthetic alloy

("desensitized state").

TABLE IX Critical energies, W^*, for sulphides nucleation as a function of temperature

Critical energy	Temperature (°C)			
	650	800	900	1000
W^* (cal cm^{-3})	8.6×10^4	12.3	0.06	37×10^{-4}
W^* (cal mol^{-1})	1.5×10^6	212	1	6.3×10^{-3}

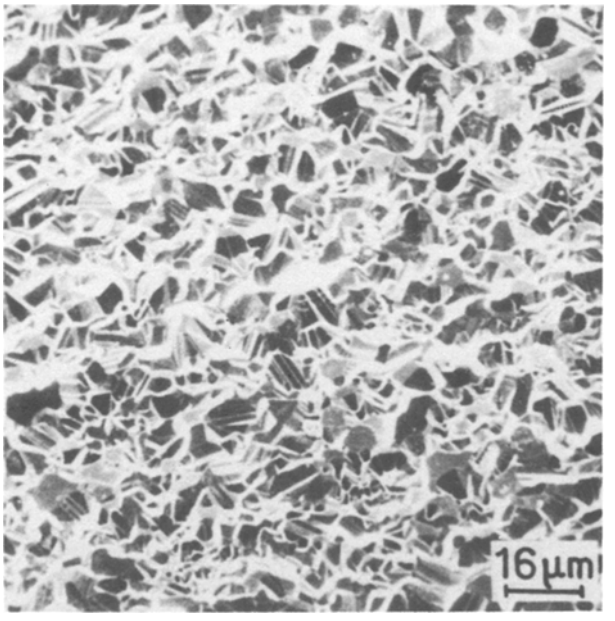

Figure 22 Morphology of the external chromium sulphide layer. Synthetic alloy in a desensitized state. Sulphidization 8 h at 800° C, $p(H_2S) = 10^{-2}$ atm.

(x is the depth, with respect to the metal surface, of the last observable chromium sulphide in the alloy).

The first law indicates chemical reaction control: the role of defects and chromium carbides, already discussed on sulphide nucleation and growth, is obviously the controlling parameter.

The second law is more complex and one must take into account the different diffusion fluxes (sulphur, chromium) to or from the surface. This will now be commented on.

6.2.2. Composition variations

The nickel and chromium contents are largely affected in the near-surface region (Fig. 25a). The chromium content variation (schematized in Fig. 25b) is in fact controlling the sulphur solubility in that region.

An analysis of the predictable sulphur solubility variations is summarized in Fig. 26. Under the external sulphide layer, the sulphur content should follow, in the absence of precipitation, the curve AB. Precipitation phenomena shift that curve

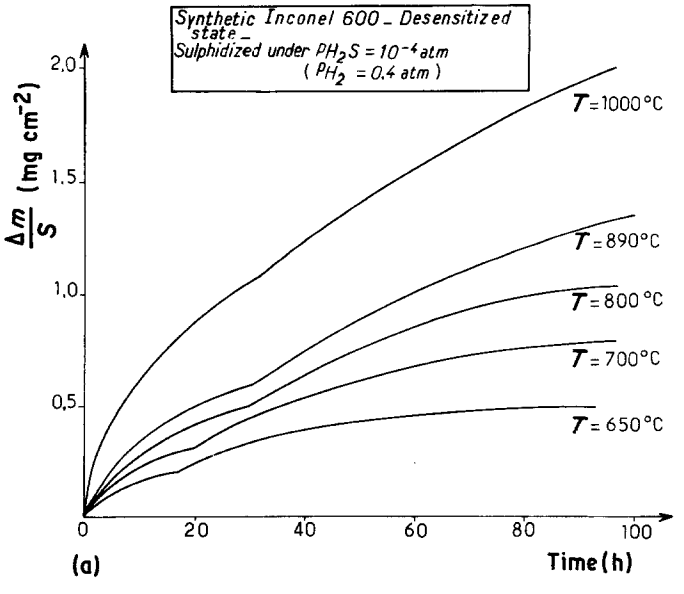

Figure 23 Parabolic shaped kinetic law for the weight gain ($\Delta m/S$) as a function of the H_2S pollution time at different temperatures. Alloys in a desensitized state.

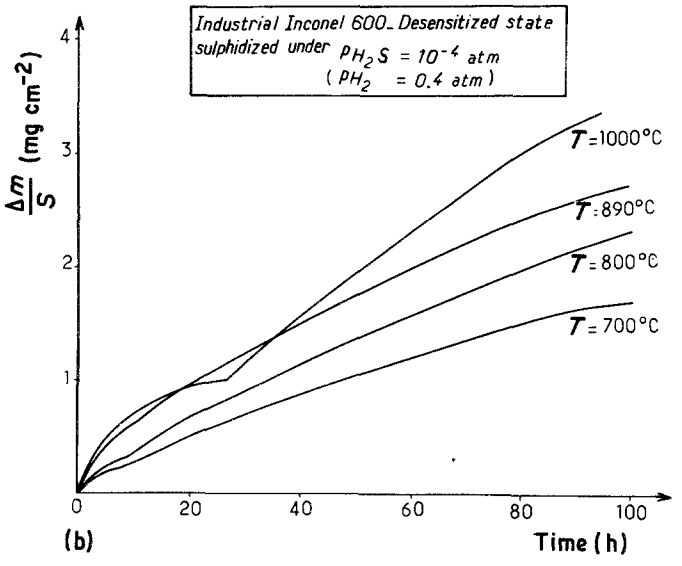

Figure 23 Continued.

toward DC. Thanks to the shape of the curve, the chromium concentration remains quasi-constant, in agreement with the plateau-shaped curve of Fig. 25 for $x \leqslant x_1$. For $x \geqslant x_1$ a usual gradient is observed.

We must also observe that the internal chromium depletion flux, to ensure the external layers growth, occurs according to a $t^{1/2}$ law.

As the internal sulphide layer is thicker than x_1, the growth law (in $t^{0.39}$) of that layer is, in fact, a consequence of both sulphur inward diffusion and sulphide nucleation rate, themselves influenced by the chromium flux.

6.2.3. Mechanical properties approach

The different sequences of internal sulphidation induce variations of the mechanical properties. These can be used as a quantitative indication of the succession of the sequences. The criterion chosen here is the flow stress for 5% elongation in tension ($\sigma 5\%$) and more precisely the evolution $\Delta\sigma 5\%$ when one compares an H_2S annealing with the same annealing under argon (Figs. 27a and b).

For sulphidization durations up to 50 h for the synthetic alloys, the chromium depletion induces plastic softening, with $t^{1/2}$ kinetics (Fig. 28). After 50 h, the hardening effect of the sulphide precipitates appears. The observed kinetic law is then a composition of the preceeding $t^{1/2}$ law and the $t^{0.39}$ law of internal sulphidation (see Section 6.2.1), leading to the shape of the experimental curve (Fig. 28).

The behaviour is quite different in the industrial alloys: the consolidation step not only appears more rapidly (30 h at 700° C), but a quasi-instantaneous hardening may often appear for the lowest sulphidizing temperature (650° C) (Fig. 29) before the plastic softening part of the chromium depletion; these effects are a consequence of the role of carbides to accelerate the nucleation of internal sulphides.

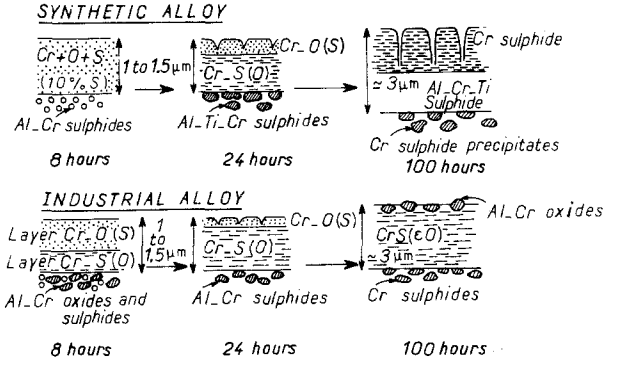

Figure 24 Scheme of the three main stages of H_2/H_2S pollution process at 750° C ($p(H_2S) = 10^{-4}$ atm and $pH_2 = 0.4$ atm) for both alloys.

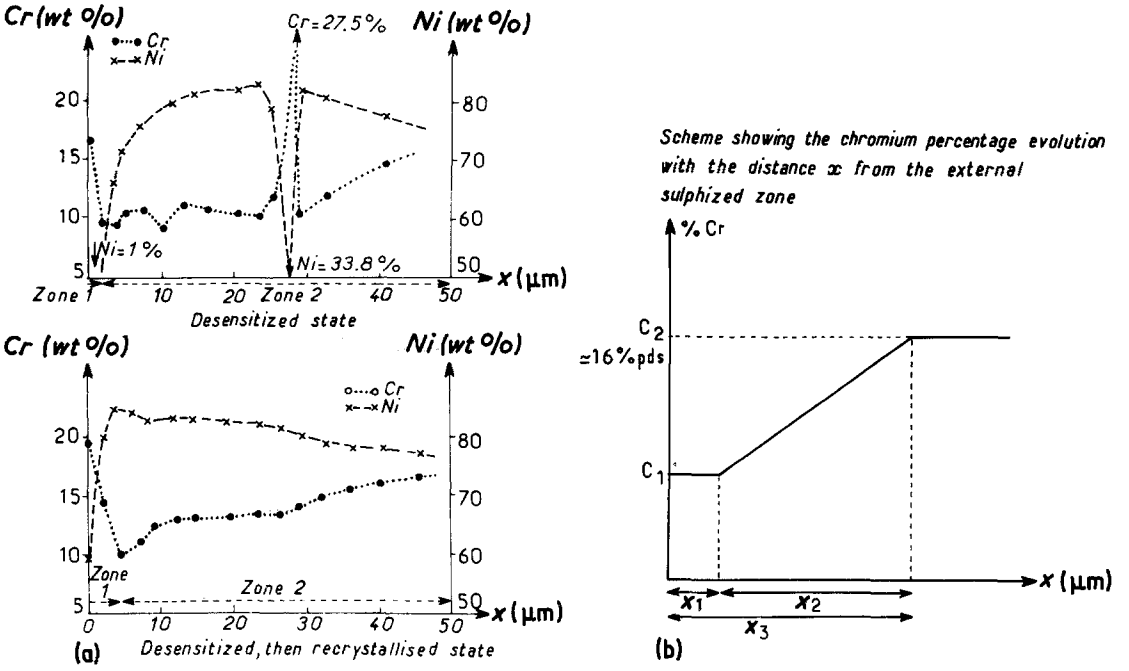

Figure 25 Experimental (a) and theoretical (b) modification of the chromium and nickel content in the sulphidized zone. Synthetic alloy in a recrystallized state, 8 h at 1000° C under $p(H_2S) = 10^{-4}$ atm.

7. Final discussion and summary

A general description of the high sulphidization process of the same alloys, including phases identification and influence of pressure and temperature have been given in another study [5]. The present results, obtained under low H_2S pressures have allowed to separate as much as possible the difference steps of the surface and internal sulphidation.

The most striking result is the influence of the defects and of the chromium carbides ($Cr_{23}C_6$) on the distribution of elementary sulphur and chromium sulphides in the bulk or on the surface of the alloys. The consequence is a modification of the sulphidizing kinetics and of the nucleation and growth of sulphide phases.

During the first step of sulphur transport through the pre-existing Cr_2O_3 scale in the metal, the diffusional aspect is predominant. In the metal microstructure, the diffusion phenomena are modified by the influence of defects (dislocations) and chromium carbides. Grain boundary diffusion and sulphur defects interactions play a major role.

Sulphur gathering as clusters is a non-equilibrium process. At the surface it can be described in terms of Cr–S interactions and decrease of the surface energy. In the metal grain boundaries, sulphur seems to be engaged in covalent S–S bond, in agreement with Loesh's model.

A competition with phosphorus segregation in industrial alloys is demonstrated.

The step of sulphide-phase nucleation is essentially controlled by the thermodynamical aspect. On the surface the usual thermodynamic formula may be used, but in the bulk of the alloy, we have

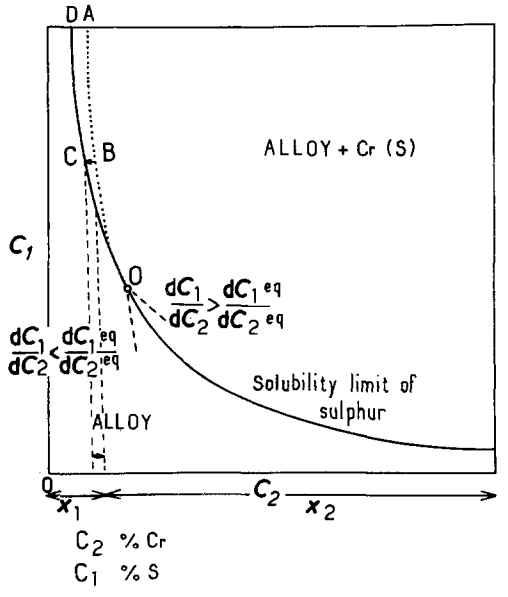

Figure 26 Experimental and theoretical solubility limit for sulphur (C_1) as a function of the chromium content (C_2) in the internal sulphidized layer.

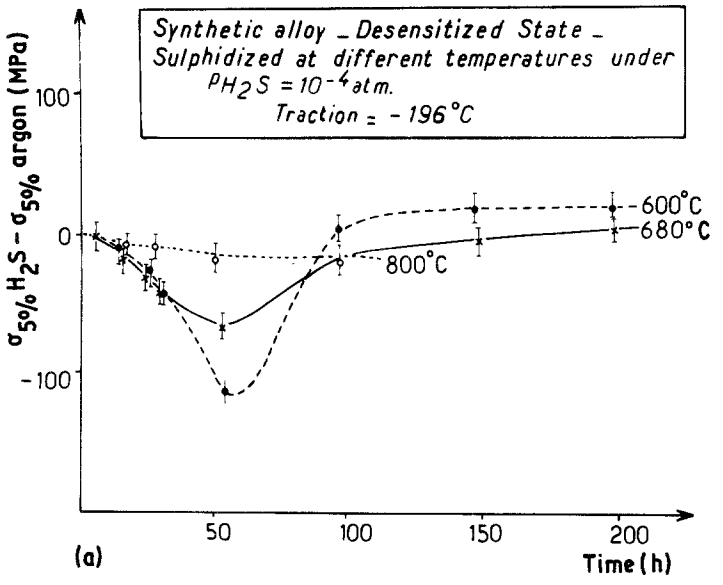

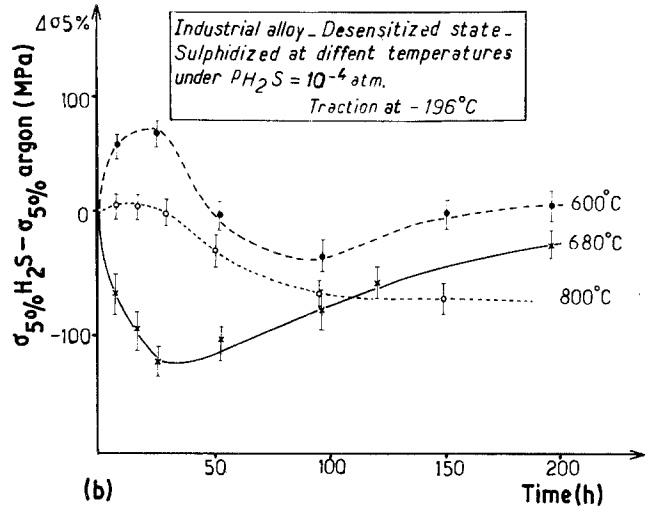

Figure 27 Experimental evolution of the $\sigma 5\%$ (H_2S)$-\sigma 5\%$ (argon) as a function of the pollution time at different temperatures, under $pH_2S = 10^{-4}$ atm ($pH_2 = 0.4$ atm).

to include Burke's criterion of precipitation induced stresses.

The role of chromium carbides is a consequence of the high chromium activity in their vicinity and of the steric and energetic gains during sulphide precipitation from carbides.

During the last step of sulphide-phase growth, the diffusional aspect again becomes more impor-

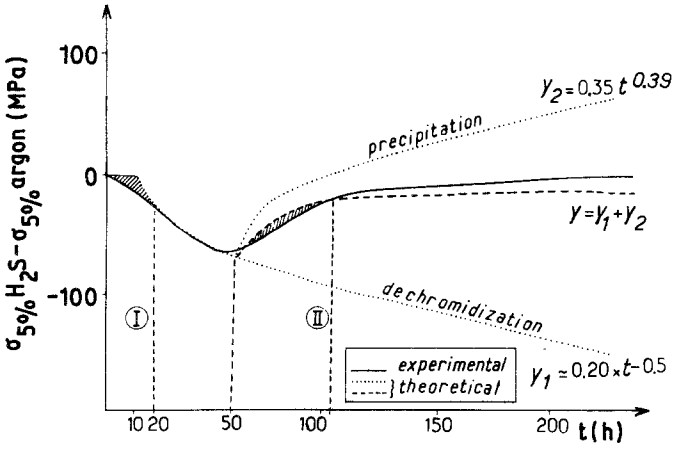

Figure 28 Decomposition of the $\Delta\sigma 5\% = f(t)$ curve of Fig. 27a by taking into account the two distinct experimental laws of: (1) dechromidization in $y_1 = 0.20t^{-0.5}$, and (2) microsulphide precipitation in $y_2 = 0.35t^{0.39}$. (Synthetic alloy in a desensitized state. Sulphidized at 680° C under $p(H_2S) = 10^{-4}$ atm.)

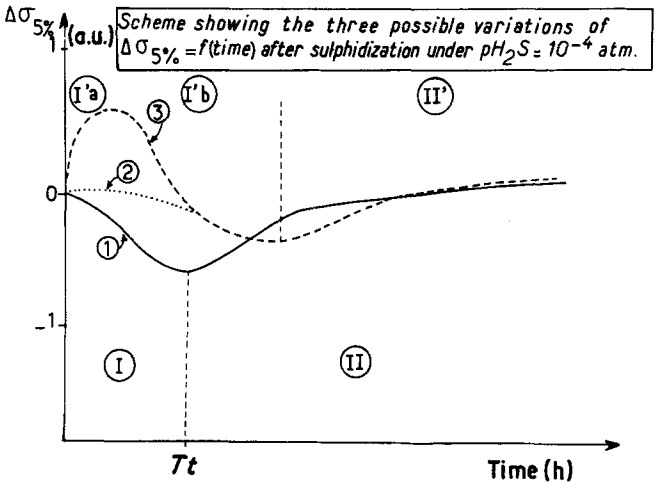

Figure 29 Analysis of the different shapes for the $\sigma 5\% = f(t)$ curves of Fig. 27b. (Industrial alloy in a desensitized state, sulphidized under $p(H_2S) = 10^{-4}$ atm.)

tant. The growth mechanism of the sulphide surface layers can be described in terms of chromium diffusion either in the scale or in the metal towards the surface. Meanwhile, the Cr_2O_3 reduction reaction has to be taken into account during a long intermediate stage. In the bulk of the alloys, the inverse fluxes of chromium towards the surface and of sulphur from the surface can explain, in combination with solubility considerations, the observed penetration laws. This step of internal sulphidation induces strong variation of the mechanical properties which can be used as a sensitive indicator of the sulphidation process.

As for the resistance of this type of alloys to sulphidizing corrosion, one practical consequence is that an even distribution of precipitates having a strong attractive effect to sulphur (as carbide) in the microstructure, can be considered as beneficial.

Acknowledgements

This study was performed partly with financial support and supply of materials from the Department Etude des Matériaux, Direction des Etudes et des Recherches de l'Electricité de France, Les Renardières. Part of the work was done with the help of Dr M. Guttmann at the Ecole des Mines de Corbeil, Miss C. Quesne, and Messrs F. Charpentier, C. Haut and B. Piccinin of our laboratory. We wish also to thank Professor R. W. Cahn for his help with the presentation of this paper.

References

1. R. A. RAPP, AGARD Report No. 120 (1972) 147.
2. P. MOULIN, F. ARMADET, G. BERANGER and P. LACOMBE, *Mem. Sci. Rev. Met.* 74 (1977) 161.
3. S. MROWEC, T. WERKER and M. ZASTAWNIK, *Corr. Sci.* 13 (1973) 677.
4. J. STRINGER, *Ann. Rev. Mater. Sci.* 7 (1977) 477.
5. G. MOULIN, M. AUCOUTURIER and P. LACOMBE, *J. Nucl. Mater.* 82 (1979) 347.
6. *Idem, ibid.* 82 (1979) 372.
7. *Idem, J. Mater. Sci.* 15 (1980) 3025.
8. J. OUDAR, *Mem. Sci. Rev. Met.* 9 (1975) 349; J. OUDAR and M. HUBER, *J. Cryst. Growth* 31 (1975) 345.
9. G. MOULIN, Thèse de Doctorat d'Etat, Orsay (1981).
10. P. DUMAS, Thèse de Doctorat d'Etat, Dijon (1979); J. M. PICHARD, M. PERDEREAU and L. C. DUFOUR, *J. Microsc. Spec. Elec.* 4 (1979) 95.
11. K. STRATER and Ch. L. MANTELL, *Trans. AIME* 230 (1964) 1141.
12. J. OUDAR, *Met. Corr. Ind.* 423 (1960) 397.
13. A. M. HUNTZ, D. MARCHIVE, M. AUCOUTURIER and P. LACOMBE, *Int. J. Appl. Radio isotop.* 30 (1979) 601.
14. G. MOULIN, J. OVEJERO-GARCIA, C. HAUT, M. DADIAN and M. AUCOUTURIER, *Rev. Met.* 11 (1978) 627.
15. A. LARERE, G. MOULIN, J. OVEJERO-GARCIA, C. HAUT and C. ROQUES-CARMES, *Scripta Metall.* 14 (1980) 703.
16. M. GUTTMANN, Ph. DUMOULIN, N. TAN TAI and P. FONTAINE, *Corr. NACE* 37 (1981) 7.
17. M. K. E. LOUDJANI, Thèse de Doctorat 3ème Cycle, Orsay (1980).
18. F. A. KROGER and H. J. VINK, *Solid State Phys.* 3 (1955) 399.
19. C. MONTY, Ecole d'Eté "Défauts Ponctuels dans les Solides", (Ed. la Revue de Physique, Confolant, 1977) p. 345.
20. N. BARBOUTH and J. OUDAR, *Scripta Metall.* 10 (1976) 415.
21. *Idem, ibid.* 6 (1972) 371.
22. F. MOYA, G. E. MOYA-GONTIER, F. CABANE-BROUTY and J. OUDAR, *Acta Metall.* 19 (1971) 1189.
23. Y. ADDA and J. PHILIBERT, "La diffusion dans les Solides" Vols. I and II, PUF (Bibliothèque des Sciences et Techniques Nucléaires, Paris, 1966).

24. M. LAGUES and J. L. DOMANGE, *Vide* **28** (1973) 100.
25. F. MOYA, Thèse de Doctorat d'Etat, Marseille (1970).
26. F. MOYA, G. E. MOYA-GONTIER and F. CABANE-BROUTY, *Phys. Status Solidi A2* **101** (1970).
27. J. B. WAGNER Jr, "Electrochemical Conductivity and Diffusion", pp. 283–301.
28. D. D. PRUTHI, M. S. ANAND and R. P. AGARVALA, *J. Nucl. Mater.* **64** (1977) 206.
29. W. C. HAGEL and A. U. SEYBOLT, *J. Electrochem. Soc.* **108** (1961) 1146.
30. M. GUTTMANN, *Surf. Sci.* **53** (1975) 213.
31. H. E. CHUANG, Z. SZKLARSKA, SMIALOWSKA and R. W. STAEHLE, *Scripta Metall.* **19** (1979) 773.
32. M. GLEITER, *Acta Metall.* **27** (1979) 1749.
33. Ph. DUMOULIN and M. GUTTMANN, *Mater. Sci. Eng.* **42** (1980) 249.
34. W. LOESH, *Acta. Metall.* **27** (1979) 1885.
35. R. P. MESSMER and C. L. BRIANT, *Phil. Mag. B* **42** (1980) 569.
36. J. BURKE, "La Cinétique des Changements de Phase dans les Métaux" (Masson, Paris, 1968).
37. J. P. HAGER and J. F. ELLIOT, *Trans. AIME* **239** (1967) 513.
38. F. D. RICHARDSON and J. H. E. JEFFES, *JISI* **6** (1952) 165.
39. I. M. LIFSHITZ and V. V. SLYOZOV, *J. Phys. Chem. Solids* **19** (1961) 35.
40. J. C. COLSON, M. LAMBERTIN and J. P. LARPIN, *Mem. Sci. Rev. Met.* **11** (1977) 687.
41. J. D. COOK and J. NUTTING, Proceedings of the Symposium of the Institute of Metals, University of Manchester, 1968 (Institute of Metals, London, 1969) Monograph 33, p. 54.
42. K. HAUFFE, "Oxidation of Metals" (Plenum Press, New York, 1965).
43. R. LALAUZE and M. SOUSTELLE, *J. Chim. Phys.* **70** (1973) 1433.

Received 13 June
and accepted 28 June 1983